Automated segmentation of the heart in high-dimensional computed tomography

Bruns, S.

Publication date
2022

CHAPTER 4

AI-based quantification of planned radiation therapy dose to cardiac structures and coronary arteries in patients with breast cancer

BASED ON: S. G. M. van Velzen, S. Bruns, J. M. Wolterink, T. Leiner, M. A. Viergever, H. M. Verkooijen, and I. Išgum. "AI-based quantification of planned radiation therapy dose to cardiac structures and coronary arteries in patients with breast cancer", *International Journal of Radiation Oncology* Biology* Physics* (2021).

Abstract

PURPOSE The purpose of this chapter is to develop and evaluate an automatic deep learning method for segmentation of cardiac chambers and large arteries, and localization of the three main coronary arteries in radiation therapy planning on computed tomography (CT). In addition, a second purpose is to determine the planned radiation therapy dose to cardiac structures for breast cancer therapy.

METHODS AND MATERIALS Eighteen contrast-enhanced cardiac scans acquired with a dual-layer-detector CT scanner were included for method development. Manual reference annotations of cardiac chambers, large arteries, and coronary artery locations were made in the contrast scans and transferred to virtual non-contrast images, mimicking non-contrast-enhanced CT. In addition, 31 non-contrast-enhanced radiation therapy treatment planning CTs with corresponding dose-distribution maps of breast cancer cases were included for evaluation. For reference, cardiac chambers and large vessels were manually annotated in two 2-dimensional (2D) slices per scan (26 scans, totaling 52 slices) and in 3-dimensional (3D) scan volumes in five scans. Coronary artery locations were annotated on 3D images. The method uses an ensemble of convolutional neural networks with two output branches that perform two distinct tasks: (1) segmentation of the cardiac chambers and large arteries and (2) localization of coronary arteries. Training was performed using reference annotations and virtual non-contrast cardiac scans. Automatic segmentation of the cardiac chambers and large vessels and the coronary artery locations was evaluated in radiation therapy planning CT with Dice similarity coefficient (DSC) and average symmetric surface distance (ASSD). The correlation between dosimetric parameters derived from the automatic and reference segmentations was evaluated with R^2.

RESULTS For cardiac chambers and large arteries, median DSC was 0.76 to 0.88, and the median ASSD was 0.17 to 0.27 cm in 2D slice evaluation. 3D evaluation found a DSC of 0.87 to 0.93 and an ASSD of 0.07 to 0.10 cm. Median DSC of the coronary artery locations ranged from 0.80 to 0.91. R^2 values of dosimetric parameters were 0.77 to 1.00 for the cardiac chambers and large vessels, and 0.76 to 0.95 for the coronary arteries.

CONCLUSIONS The developed and evaluated method can automatically obtain accurate estimates of planned radiation dose and dosimetric parameters for the cardiac chambers, large arteries, and coronary arteries.

4.1 Introduction

Radiation exposure of the heart during radiation therapy treatment for breast cancer is known to increase the risk of ischemic heart disease (IHD).[1] Multiple studies have reported an increased risk of IHD with increasing mean heart dose (MHD);[1] however, the dose distribution within the heart is not homogeneous. A study by Jacob *et al.*[2] showed that the dose delivered to the left ventricle and the three main coronary arteries can differ substantially from the MHD. Van den Bogaard *et al.*[3] showed that replacing the MHD in a prediction model by the dose to the left ventricle improved prediction of acute coronary events. Moreover, previous research has shown that a high dose to the coronary arteries could lead to an increased risk of stenosis in these arteries.[4,5]

Taking the irradiation dose to specific heart structures into account during radiation therapy treatment planning can help to mitigate radiation-induced cardiac damage and to reduce the risk of IHD.[2] However, computed tomographic (CT) scans used for radiation therapy treatment planning are acquired without contrast agent and without electrocardiograph (ECG) triggering. Hence, visualization of cardiac chambers and the coronary arteries is suboptimal, which makes manual delineation of those structures practically infeasible. On the other hand, cardiac structures can be visualized with high accuracy in coronary CT angiography (CCTA) scans. Therefore, Jacob *et al.*[2] used image registration to transfer delineations made in CCTA scans to the planning CT image.[2] However, CCTA is not part of routine clinical care for patients with breast cancer. Accordingly, cardiac contouring atlases have been developed in non-contrast CT for reproducible manual contouring. Moreover, automatic methods have been proposed that use registration of non-contrast CT atlases to delineate cardiac structures on the planning CT scan.[6–8]

These previous methods focus on the delineation of cardiac chambers. Few methods have been proposed to segment the coronary arteries in non-contrast-enhanced CT scans. Van den Bogaard *et al.*[9] derived a segmentation of the left anterior descending artery based on anatomic landmarks and prior segmentation of the left and right ventricle. Morris *et al.*[10] proposed to use additional information from magnetic resonance imaging scans to develop a method for segmentation of both the cardiac chambers and the three main coronary arteries.

Recently proposed machine learning methods use training data to learn to segment cardiac structures. The accuracy of the reference standard used for training in previous methods is often limited by the lack of contrast or inaccuracies owing to intra-patient registration. Recently, Bruns *et al.*[11] proposed to obtain reference segmentation in contrast-enhanced CT acquired with a dual-layer detector CT scanner. By leveraging the dual-energy information of such scans, the reference annotations can be transferred to perfectly aligned virtual non-contrast (VNC) CT images, mimicking non-contrast-enhanced CT images. This way, a deep learning segmentation method could be trained using reference segmentations with voxel-level accuracy, which showed excellent

performance in the segmentation of cardiac chambers and large arteries in non-contrast-enhanced cardiac CT images.

A robust segmentation algorithm could facilitate large-scale studies investigating the consequences of the dose planned to cardiac structures and coronary arteries in radiation therapy for breast cancer. Hence, the purpose of this chapter was to develop and evaluate a deep learning method for the segmentation of cardiac structures in treatment planning CT scans to allow the calculation of dosimetric parameters in patients with breast cancer. In this chapter, we build on work by Bruns *et al.*[11] to develop a deep learning method for segmentation of cardiac chambers and large arteries, and for localization of the trajectories of the three major coronary arteries in planning CT scans. We evaluate the quality of the obtained segmentations and whether these provide accurate dosimetric parameters compared with manually defined segmentations.

4.2 Methods and materials

4.2.1 Data

To develop the segmentation method, 18 CCTA scans from the CLARITY study were included[12] (Fig. 4.1). Scans were acquired on a dual-layer-detector CT scanner (IQon; Philips Healthcare, Best, The Netherlands) using 120 kVp and 120 mAs. Scans were reconstructed to 0.35 to 0.50 mm in-plane resolution and 0.9 mm slice thickness. With the dual-energy information, a CCTA and a VNC image resembling a non-contrast-enhanced CT could be reconstructed from a single contrast-enhanced acquisition. To obtain a reference standard for training of a deep learning method, the cardiac structures and three main coronary arteries were segmented in the CCTA scans. Reference segmentations of the cardiac chambers and large arteries were made in a semiautomatic manner as described by Bruns *et al.*[11] and included the left ventricle myocardium, left ventricle blood pool (LVBP), right ventricle (RV), left atrium (LA), right atrium (RA), ascending aorta, and pulmonary artery trunk. Initial segmentations in contrast-enhanced images were obtained using a previously described algorithm.[13] Subsequently, a medical student performed manual voxel-wise correction of the initial segmentations. Thereafter, all reference segmentations were verified and then corrected by a resident if necessary (7 years' experience in cardiothoracic imaging). To obtain reference segmentations of the coronary arteries, we used an automatic method for tracking coronary arteries in the CCTA scans.[14] Subsequently, an observer (4 years' experience) selected the main branches of the left anterior descending (LAD), left circumflex (LCX), and right coronary artery (RCA), verified the segmentations and then manually corrected them if necessary.

The evaluation set comprised 31 radiation therapy treatment planning CT scans of patients from clinical practice (Fig. 4.1). Scans were acquired without contrast enhancement, without ECG triggering, during free breathing, and with 120 kVp. Scans

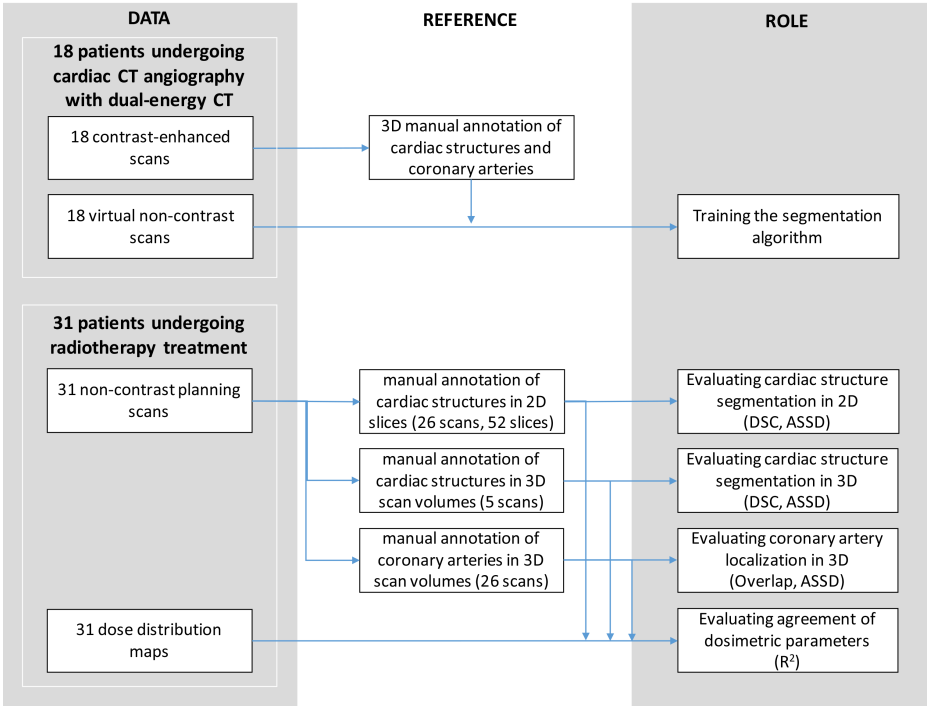

Figure 4.1: Overview of the data and manual annotations used in the study. Abbreviations: DSC = Dice similarity coefficient; ASSD = average symmetric surface distance.

were reconstructed to 0.78 to 1.37 mm in-plane resolution, 3 mm slice thickness, and 3 mm slice spacing. Dose distribution maps and manual contours were obtained from the radiation therapy treatment planning software used in the clinic. Manual contours included the whole heart without subdivision into separate cardiac structures. Three-dimensional (3D) CT radiation therapy treatment planning was performed using Monaco (Elekta; 2016). Because all data regarding breast cancer patients were collected retrospectively and anonymously, the need for informed consent was waived by the local institutional review board.

Manual segmentation of the cardiac structures was performed to define the reference standard for evaluation. Because of the lack of contrast in the radiation therapy treatment planning CT images, voxel-wise manual segmentation of the whole 3D volume is extremely time consuming.[11] To maximize the number of scans, and thus maximize anatomic variation in the test set, segmentations were made in a set of 2-dimensional (2D) axial slices of the heart selected from 26 scans. Two slices per scan were randomly selected using the clinical whole heart delineations, totaling 54 slices. This way, the whole heart was likely covered by the included slices. Apical slices were manually excluded and replaced with a new randomly chosen slice because, in those slices, the heart was poorly visible.

Given time-consuming manual annotation in 3D imaging, and the need to evaluate the automatic method to ensure full heart coverage, five scans were also annotated manually in 3D using voxel-wise annotation of cardiac structures. The reference for artery localization was set by drawing the centerlines of the three main coronary arteries in each 3D image volume.

4.2.2 Segmentation of cardiac structures

We built on a method that was proposed for the segmentation of cardiac chambers and large arteries in non-contrast-enhanced ECG-synchronized cardiac CT imaging.[11] Cardiac structures are generally poorly visible in non-contrast-enhanced CT scans, which renders manual segmentation a practically infeasible task. CT scans with a contrast agent, however, clearly visualize all of these structures and facilitate their segmentation. Hence, to segment cardiac chambers and large arteries in non-contrast-enhanced CT, we trained the method using VNC CT images (Fig. 4.2A, Training). Owing to voxel-wise correspondence, the reference segmentations and artery locations made on the contrast-enhanced image were transferred directly with voxel accuracy to the VNC image for training. Because VNC images closely resemble conventional non-contrast-enhanced CT images, the trained method can be used for segmentation of conventional non-contrast-enhanced CT images. After training, the method was applied to non-contrast-enhanced planning CT images (Fig. 4.2A, Testing).

Our network performed two distinct tasks: segmentation of the cardiac chambers and large arteries and localization of the coronary arteries. The coronary arteries are

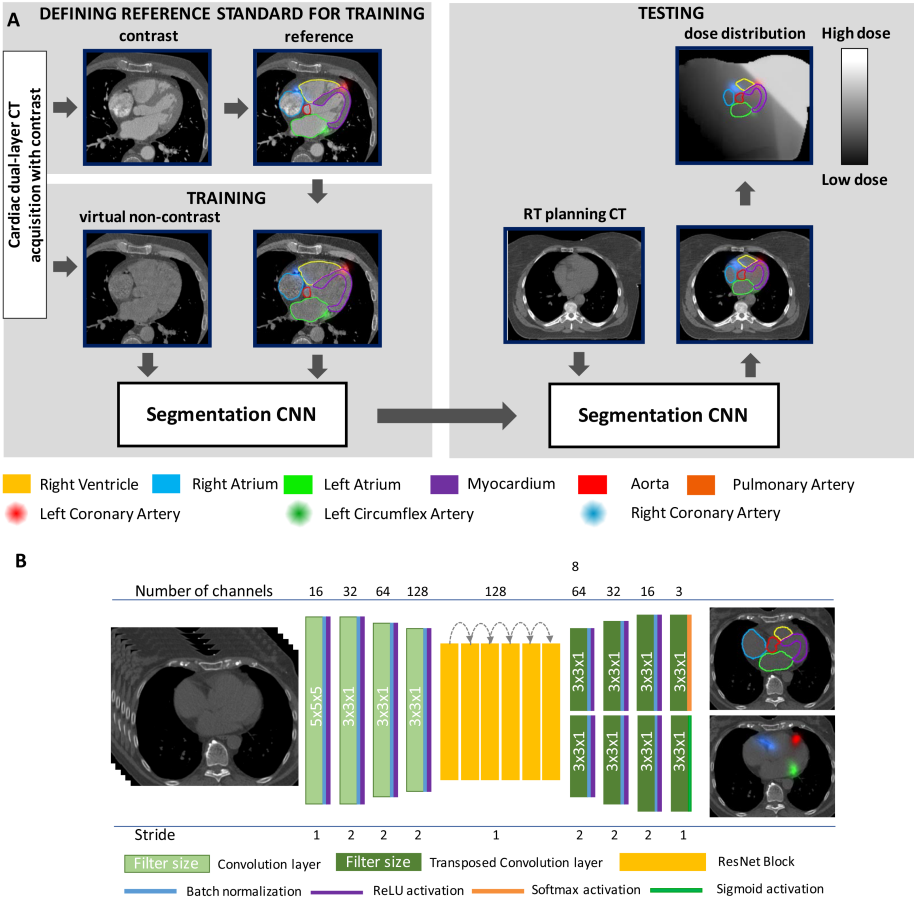

Figure 4.2: (A) Schematic overview of the deep learning segmentation method. The method is trained using virtual non-contrast scans with the manually determined reference. Thereafter, the method is applied to planning CT scans. The segmentations and artery locations are then transferred to the dose distribution map to calculate dose parameters. (B) The CNN architecture uses two separate output paths that perform two distinct tasks: (1) segmentation of cardiac chambers and large arteries, and (2) localization of the coronary arteries. Abbreviations: CNN = convolutional neural network; CT = computed tomography.

small structures compared with the other heart structures and are barely visible in non-contrast-enhanced CT, especially in non–ECG-triggered scans. Hence, simply adding the arteries to the segmentation maps would pose a challenging problem because of class imbalance. Therefore, we designed a 3D convolutional neural network (CNN) with two output branches, a branch for structure segmentation and a branch for localizing the coronary arteries. Contrary to the branch that segments cardiac structures, the artery localization branch does not predict voxel labels but predicts, per voxel, the squared inverse distance to the target artery segmentation using regression.[15] This condition renders a heatmap-like prediction of the artery trajectories. For training, we converted the reference segmentation of the coronary arteries to a heatmap by applying an inverse Euclidean distance transform.

Inspired by the method of Bruns *et al.*,[11] the CNN architecture used in this chapter consists of an encoding path, which is connected to the output branches by six ResNet[16] blocks that exploit skip connections for optimal information propagation (Fig. 4.2B). The architecture is relatively small to ensure optimal network learning from a limited data set. Because an ensemble of CNNs provides more robust predictions than a single CNN,[17] the final segmentation method consists of an ensemble of 18 CNNs.[11] The data set of VNC images is randomly divided into six folds with 15 scans for training and three for validation. In each fold, three CNNs are trained with different random initializations, totaling 18 CNNs. The input of the CNNs consists of slabs, consisting of five stacked axial image slices of 256 × 256 voxels. For optimal performance in the target CT images, the VNC images are resampled to the average resolution of the radiation therapy planning CTs — namely, 1 mm in-plane resolution and 3 mm slice spacing. All 18 CNNs are trained for 10,000 iterations with minibatches of 32 randomly sampled image slabs, using Adam[18] for optimization. The loss function for segmentation of the cardiac chambers and large arteries is defined as the negative sum of soft Dice similarity coefficients over all classes. In addition, for the coronary artery localization, an L1 loss of the predicted heatmap with the reference heatmap is calculated. For more details regarding the training, we refer to Bruns *et al.*[11] To obtain the final prediction, predictions of all 18 CNNs are averaged. From the coronary artery heatmaps, centerlines are extracted. After training, the method was applied to the test scans fully automatically, and manual correction of the segmentation results was performed.

4.2.3 Quantitative evaluation

To evaluate the performance of the segmentation algorithm, the automatic segmentations and artery trajectory locations were compared with the manual reference. Segmentations of the cardiac chambers, aorta, and pulmonary artery were evaluated using the Dice similarity coefficient (DSC). The DSC reflects the overlap of two segmentations, with a DSC of 1.0 reflecting perfect agreement. The DSC is less appropriate

for the evaluation of small structures such as the coronary arteries. Therefore, similar to the DSC, the overlap with the reference was used, defined as the harmonic mean between recall and precision.[19] A distance threshold was used to define true-positive, true-negative, false-positive, and false-negative centerline locations. The automatic location was defined as true positive if its distance to the reference location was smaller than the predefined distance threshold. Two thresholds were evaluated, set to 0.7 cm and 1.0 cm. Moreover, the average symmetric surface distance (ASSD), which measures the average distance between two segmentations, was used to evaluate the structure segmentations and coronary artery locations. An ASSD of 0.0 cm reflects perfect agreement of segmentations.

Dosimetric parameters derived from the automatic segmentations were compared with those derived from manual reference segmentations. By combining the automatically and manually obtained segmentations of each anatomic structure with the dose distribution maps, we calculated dosimetric parameters for the structures of interest (Fig. 4.2A, Testing). For evaluated axial slices, the D_{mean} (mean dose) expressed in Grays (Gy), V_{1Gy} (percentage of the volume of a structure receiving 1 Gy or more), and $D_{5\%}$ (the mean dose to the 5% of the structure that receives the highest dose) were calculated for each manually and automatically segmented heart structure. Correlation between the automatically and the manually derived dosimetric parameters was assessed using R^2 of the linear regression.

4.3 Results

4.3.1 Segmentation of cardiac chambers and large arteries

The DSC overlap between automatic and manual segmentations varied between the different structures (Table 4.1). The highest DSC was observed for the LVBP and the aorta, with a median of 0.88 (interquartile range [IQR], 0.85–0.90) and 0.88 (IQR, 0.83–0.92), respectively. The myocardium had the lowest DSC among cardiac structures (median of 0.76 [IQR, 0.68–0.80]), which is also the most challenging to segment in non-contrast-enhanced images. The ASSD ranged from 0.17 to 0.27 cm over the different structures.

Table 4.1: Performance of segmentation and correlation of derived dosimetric parameters.

Evaluation	BP	RV	LA	RA	MYO	AO	PUL
Segmentation							
2D slices data set							
Median DSC	0.88	0.85	0.84	0.82	0.76	0.88	0.86
(IQR)	(0.85–0.90)	(0.77–0.89)	(0.74–0.87)	(0.75–0.90)	(0.68–0.80)	(0.83–0.92)	(0.77–0.90)
Median ASSD	0.27	0.25	0.26	0.24	0.22	0.17	0.20
(IQR) (cm)	(0.22–0.30)	(0.21–0.33)	(0.21–0.31)	(0.18–0.34)	(0.18–0.26)	(0.14–0.24)	(0.13–0.45)
3D data set							
Median DSC	0.93	0.91	0.92	0.92	0.87	0.91	0.90
(IQR)	(0.91–0.93)	(0.90–0.93)	(0.90–0.93)	(0.90–0.93)	(0.86–0.88)	(0.90–0.93)	(0.88–0.91)
Median ASSD	0.08	0.08	0.08	0.07	0.07	0.10	0.07
(IQR) (cm)	(0.07–0.08)	(0.08–0.11)	(0.07–0.08)	(0.06–0.08)	(0.06–0.08)	(0.08–0.10)	(0.06–0.08)
Correlation dosimetric parameters (R^2)							
2D slices data set							
D_{mean}	0.99	0.77	0.94	0.95	0.97	0.91	0.83
$D_{5\%}$	0.99	0.86	0.99	0.93	0.99	0.99	0.77
V_{1Gy}	0.97	0.82	0.94	0.93	0.99	0.93	0.91
3D data set							
D_{mean}	1.00	1.00	1.00	1.00	1.00	1.00	0.99
$D_{5\%}$	1.00	1.00	1.00	1.00	1.00	1.00	0.99
V_{1Gy}	1.00	1.00	1.00	1.00	1.00	1.00	1.00
Mean absolute difference dosimetric parameters							
2D slices data set							
D_{mean}(Gy)	0.08	0.31	0.14	0.14	0.21	0.19	0.30
$D_{5\%}$(Gy)	0.24	0.97	0.15	0.20	0.72	0.26	0.51
V_{1Gy}	2%	8%	1%	5%	2%	1%	3%

Abbreviations: 2D = 2-dimensional; 3D = 3-dimensional; AO = aorta; ASSD = asymmetric surface distance; BP = left ventricular blood pool; $D_{5\%}$ = the mean dose to the 5% of the structure that receives the highest dose; D_{mean} = mean dose; DSC = Dice similarity coefficient; IQR = interquartile range; LA = left atrium; MYO = left ventricular myocardium; PUL = pulmonary artery: RA = right atrium; RV = right ventricle; V_{1Gy} = percentage of the volume of a structure receiving 1 Gy or more.

Evaluation in the five scans fully segmented in 3D imaging found a DSC between 0.87 and 0.93 for the different structures (Table 4.1), which is higher for every evaluated structure than the DSC that was found in 2D imaging. Moreover, the ASSD is substantially lower in the 3D evaluation.

4.3.2 Coronary artery localization

The observed median ASSD was 0.37 cm (IQR, 0.28–0.73 cm), 0.56 cm (IQR, 0.44–0.67 cm) and 0.51 cm (IQR, 0.40–0.69 cm) for the LAD, RCA, and LCX, respectively (Fig. 4.3B). The artery localization was within 1.0 cm of the reference with a median overlap of 0.91, 0.81, and 0.80 cm for the LAD, RCA, and LCX, respectively. Median overlap for 0.7 cm was 0.79, 0.55, and 0.59 cm for the LAD, RCA, and LCX, respectively.

4.3.3 Dosimetric parameters

The agreement between dosimetric parameters derived from the automatically generated segmentations, and the dosimetric parameters derived from manual segmentations are shown in Figure 4.4. The R^2 values of D_{mean} were >0.90 for the LVBP, LA, RA, MYO, and AO (Table 4.1). For the RV and pulmonary artery, these values were 0.77 and 0.83, respectively. The R^2 values for the $D_{5\%}$ and V_{1Gy} ranged between 0.99 and 0.77 and can be found in Table 4.1. Evaluation in the five scans annotated in 3D imaging showed a high correlation for all dosimetric parameters for all structures (Table 4.1).

The agreement of D_{mean} derived from automatically and manually located arteries was high, with R^2 values of 0.86, 0.93, and 0.95 for the LAD, RCA, and LCX, respectively (Table 4.2). R^2 values for the $D_{5\%}$ and V_{1Gy} ranged from 0.76 to 0.94. Figure 4.5 shows representative dose-volume histograms obtained with the automatic and manual segmentations and artery locations. The DSC, overlap, and ASSD indicate the presence of imperfections in the segmentations and artery locations. Despite the imperfections, the doses received by the automatically and manually derived segmentations and locations were similar.

4.4 Discussion

In this chapter, we developed and evaluated a method for fully automatic segmentation of heart chambers and large arteries and localization of the coronary arteries in non-contrast-enhanced radiation therapy planning CT scans. The method consists of an ensemble of CNNs that was trained with VNC images using multispectral characteristics of the scans made with a dual-layer CT scanner. The results show good agreement between automatic and manual reference segmentations and artery locations. An analysis of dosimetric parameters showed that the proposed method can generate accurate measurements showing the planned radiation therapy dose to each evaluated structure.

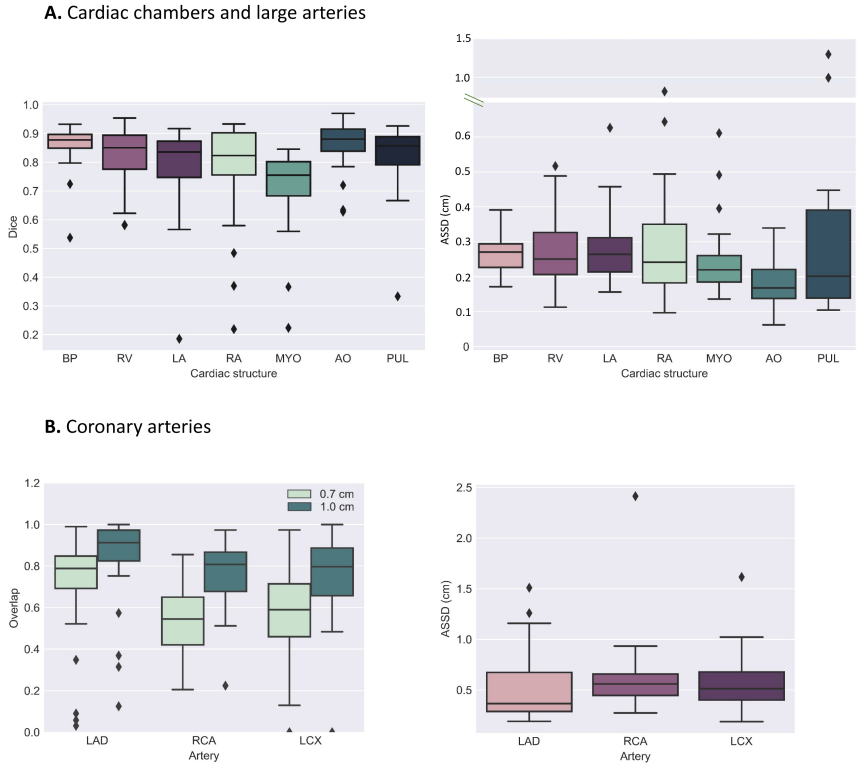

Figure 4.3: (A) Dice similarity coefficient and average symmetric surface distance for the left ventricular blood pool (BP), right ventricle (RV), left atrium (LA), right atrium (RA), left ventricle myocardium (MYO), aorta (AO), and pulmonary artery (PUL). (B). Overlap and ASSD for the left anterior descending (LAD), left circumflex (LCX) and right coronary artery (RCA).

Table 4.2: Performance of artery localization and correlation of derived dosimetric parameters.

Evaluation	LAD	RCA	LCX
Localization			
Median overlap 1.0 cm (IQR)	98% (83%–100%)	88% (70%–100%)	80% (67%–87%)
Median ASSD, cm (IQR)	0.37 (0.28–0.73)	0.56 (0.44–0.67)	0.51 (0.40–0.69)
Correlation dosimetric parameters (R^2)			
D_{mean}	0.86	0.93	0.95
$D_{5\%}$	0.76	0.85	0.94
V_{1Gy}	0.94	0.93	0.92
Mean absolute difference dosimetric parameters			
D_{mean} (Gy)	0.86	0.93	0.95
$D_{5\%}$ (Gy)	0.76	0.85	0.94
V_{1Gy}	6%	7%	7%

Abbreviations: ASSD = asymmetric surface distance; $D_{5\%}$ = the mean dose to the 5% of the structure that receives the highest dose; D_{mean} = mean dose; IQR = interquartile range; LAD = left anterior descending; LCX = left circumflex; RCA = right coronary artery; V_{1Gy} = percentage of the volume of a structure receiving 1 Gy or more.

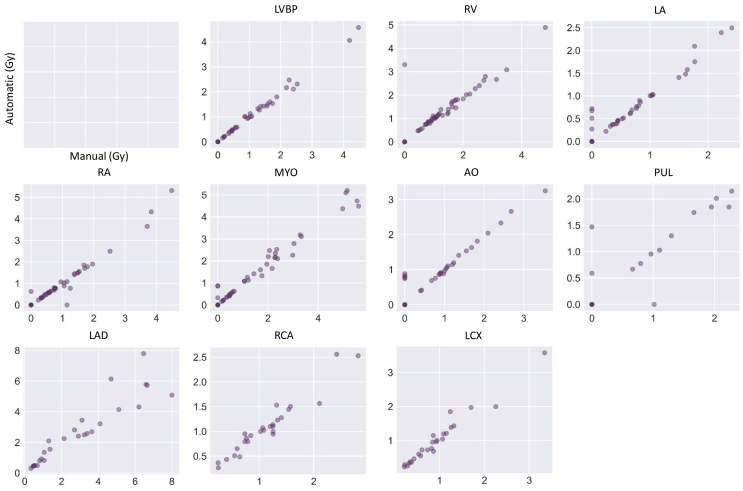

Figure 4.4: Comparison of the mean dose (D_{mean}) derived from manual and automatic structure segmentations and artery locations. Plots show the D_{mean} for the left ventricular blood pool (LVBP), right ventricle (RV), left atrium (LA), right atrium (RA), left ventricular myocardium (MYO), aorta (AO), pulmonary artery (PUL), left anterior descending artery (LAD), right coronary artery (RCA), and left circumflex artery (LCX).

For the development of the deep learning segmentation method, a set of CT scans acquired with a dual-layer-detector CT scanner was used. Because of the dual-energy properties of these acquisitions, virtual non-contrast scans can be reconstructed from an acquisition with contrast. Reference segmentations were made using the CCTA images, where visibility of the cardiac structures is optimal. Thereafter, reference segmentations were transferred with voxel level accuracy to the virtual non-contrast images, resulting in a highly accurate training reference. Previous methods evaluating radiation therapy dose to cardiac structures used both a radiation therapy planning CT and a CCTA scan to segment cardiac structures through intra-patient registration,[2,20] which is limited by the accuracy of the challenging registration between images with and without contrast enhancement. A different approach performs automatic atlas-based contouring of cardiac structures directly on the planning CT, without using a CCTA scan for contouring in between.[7,8,21] However, cardiac structures are barely differentiable on non-contrast-enhanced CT, making the atlas subject to inter-observer variability. In addition, inter-patient registration is highly challenging in images where the structure boundaries are poorly visible. Moreover, because of the lack of contrast, the performance in small structures, such as the coronary arteries, is often suboptimal.[7,8,22]

Recently, Morris *et al.*[10] proposed to use information from magnetic resonance imaging scans for the segmentation of cardiac structures and coronary arteries in radiation

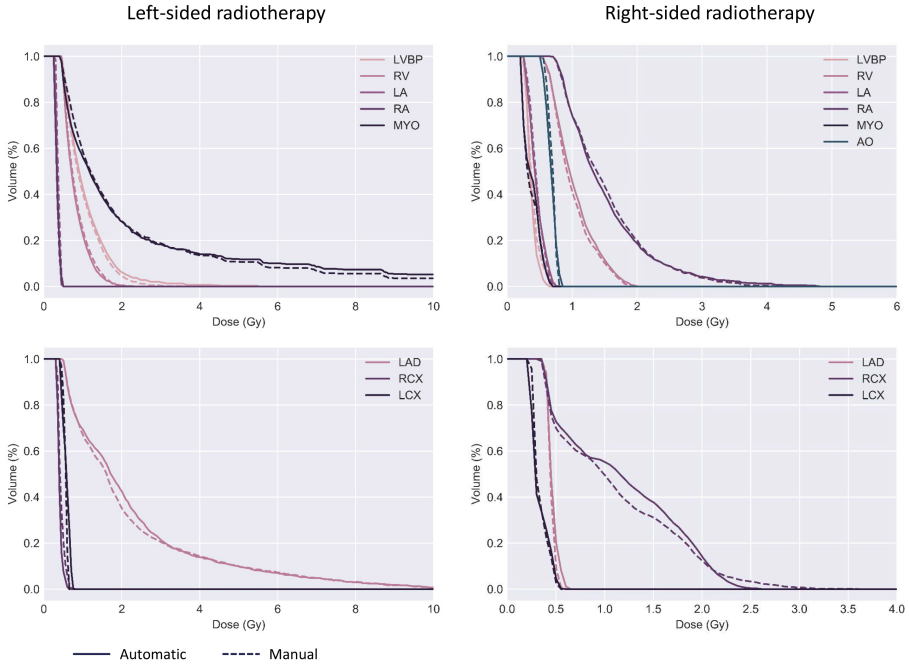

Figure 4.5: Dose-volume histograms derived from manual and automatic structure segmentations and artery locations for a patient with right- and left-sided breast cancer. Not all structures are present in the evaluated slices. The histograms show the left ventricular blood pool (LVBP), right ventricle (RV), left atrium (LA), right atrium (RA), left ventricular myocardium (MYO), aorta (AO), left anterior descending artery (LAD), right coronary artery (RCA), and left circumflex artery (LCX).

therapy planning CT scans. Compared with that study, we have achieved comparable DSC scores for the cardiac structures: 0.76–0.88 in our study when evaluated in 2D slices and 0.87–0.93 when evaluated in 3D volumes, compared with 0.77–0.88 in the 3D evaluation by Morris *et al.*[10] These results show that deep learning methods are capable of learning the complex segmentation task, despite poor contrast in the target scans.

In addition, we have evaluated the accuracy of automatically calculated dosimetric parameters. Our analysis shows that, despite small deviations from the manual reference, the automatic segmentations can provide dose parameters that have a high correlation with reference parameters. Because the coronary arteries are relatively small structures, the geometric overlap (DSC) may be low, whereas the calculated dose parameters show a high correlation with the reference.[21] Moreover, despite the DSC and ASSD scores showing that small imperfections of the automatic segmentations are present, the dose-volume histograms of the automatic and manual segmentations are similar.

In a 2D evaluation, the vast majority of the slices show a high DSC and low ASSD, but several outliers are present (Fig. 4.4). Similarly, outliers are present in the evaluation of dosimetric parameters; these are partly due to the evaluation in 2D image slices. For instance, the transition from the pulmonary artery to the right ventricle is often not well visible, which causes uncertainty in the reference annotations in the slices located in the vicinity of this transition. Moreover, on the boundary of a structure partial volume effects make it poorly visible and manual segmentation of a structure on a voxel level is prone to large inter-observer variability.[23] These uncertainties along the boundaries of structures are less pronounced in 3D evaluation; this is reflected in our results by higher DSC and lower ASSD in the five scans used for 3D evaluation. Overall, the results show that the automatic segmentation shows good agreement with the manual reference.

Because the planning CT scans used in this chapter are acquired without ECG synchronization, substantial partial volume effect and cardiac motion are visible in the scans; this could affect the myocardium and coronary arteries.[24] With current treatment technology, cardiac motion is not monitored or managed during irradiation treatment. Our presented method that segments cardiac structures could allow cardiac motion to be incorporated into margins for each cardiac structure and coronary artery during treatment planning.

The presented automatic method was trained with a relatively small data set, which might lead to limited robustness in regard to anatomic variation and unseen pathology. Therefore, we subsequently applied the method in a large set to evaluate performance in a set comprising larger diversity in anatomic variation. The results demonstrate that our method generalizes well to these variations in the evaluated set. Nevertheless, future work should focus on evaluating the method in a data set comprising other target populations and diversity in image acquisition.

In the current study, the automatic segmentation algorithm is evaluated in a group of

patients with breast cancer. However, segmentation of cardiac structures and coronary arteries could also be valuable in patients receiving radiation therapy for other types of cancer. For example, an increased risk of heart disease owing to radiation therapy has been observed in patients undergoing treatment for non-Hodgkin lymphoma,[25] and cardiac radiation exposure is associated with major adverse cardiac events in patients with non-small cell lung cancer.[26] Incorporating cardiac structures and coronary arteries into treatment planning for this or other patient groups could also be beneficial for cardiac sparing. Because CT scanning parameters and dose distributions can differ per type of irradiated cancer, careful evaluation of the segmentation results and dosimetric parameters would be needed. Moreover, to obtain better insight in radiation-related risk per cardiac structure and to determine their specific dose constraints, future research focusing on these topics is warranted.

This chapter has several limitations to consider. First, reference segmentations for evaluation were made in CT scans acquired without intravenous contrast and without ECG synchronization, which might have affected the reproducibility and accuracy of the reference segmentations. Despite this potential source of variation, we found good agreement between automatic and manual segmentations. This finding is in line with an earlier study by Bruns *et al.*[11] in which the segmentation algorithm produced accurate segmentations in a set of cardiac patients for whom both contrast and non-contrast-enhanced CT scans were available. Second, evaluation of the cardiac structure segmentations in 2D axial slices might have magnified disagreement along the border of structures. This may be less pronounced if 3D volumes were segmented for evaluation. However, 2D slice evaluation enabled the use of a larger data set comprising more anatomic variability than other studies.

4.5 Conclusion

The evaluated automatic method is an effective tool for obtaining estimates of planned radiation dose and dosimetric parameters for each cardiac chamber, large arteries, and coronary arteries. This chapter presents a step toward more detailed and spatially distributed dose planning considering the detailed anatomy of the heart. The method can facilitate large-scale studies researching the effect of radiation dose on cardiac structures and coronary arteries.

References

[1] S. C. Darby, M. Ewertz, P. McGale, A. M. Bennet, U. Blom-Goldman, D. Brønnum, C. Correa, D. Cutter, G. Gagliardi, B. Gigante, et al. "Risk of ischemic heart disease in women after radiotherapy for breast cancer", *New England Journal of Medicine*, vol. 368 (2013), pp. 987–998.

[2] S. Jacob, J. Camilleri, S. Derreumaux, V. Walker, O. Lairez, M. Lapeyre, E. Bruguière, A. Pathak, M.-O. Bernier, D. Laurier, et al. "Is mean heart dose a relevant surrogate parameter of left ventricle and coronary arteries exposure during breast cancer radiotherapy: a dosimetric evaluation based on individually-determined radiation dose (BACCARAT study)", *Radiation Oncology*, vol. 14 (2019), p. 29.

[3] V. A. van den Bogaard, B. D. Ta, A. van der Schaaf, A. B. Bouma, A. M. Middag, E. J. Bantema-Joppe, L. V. van Dijk, F. B. van Dijk-Peters, L. A. Marteijn, G. H. de Bock, et al. "Validation and modification of a prediction model for acute cardiac events in patients with breast cancer treated with radiotherapy based on three-dimensional dose distributions to cardiac substructures", *Journal of Clinical Oncology*, vol. 35 (2017), p. 1171.

[4] G. Nilsson, L. Holmberg, H. Garmo, O. Duvernoy, I. Sjögren, B. Lagerqvist, and C. Blomqvist. "Distribution of coronary artery stenosis after radiation for breast cancer", *Journal of clinical oncology*, vol. 30 (2012), pp. 380–386.

[5] C. R. Correa, H. I. Litt, W.-T. Hwang, V. A. Ferrari, L. J. Solin, and E. E. Harris. "Coronary artery findings after left-sided compared with right-sided radiation treatment for early-stage breast cancer", *Journal of clinical oncology*, vol. 25 (2007), pp. 3031–3037.

[6] M. Feng, J. M. Moran, T. Koelling, A. Chughtai, J. L. Chan, L. Freedman, J. A. Hayman, R. Jagsi, S. Jolly, J. Larouere, et al. "Development and validation of a heart atlas to study cardiac exposure to radiation following treatment for breast cancer", *International Journal of Radiation Oncology* Biology* Physics*, vol. 79 (2011), pp. 10–18.

[7] N. Maffei, L. Fiorini, G. Aluisio, E. D'Angelo, P. Ferrazza, V. Vanoni, F. Lohr, B. Meduri, and G. Guidi. "Hierarchical clustering applied to automatic atlas based segmentation of 25 cardiac sub-structures", *Physica Medica*, vol. 69 (2020), pp. 70–80.

[8] F. Duane, M. C. Aznar, F. Bartlett, D. J. Cutter, S. C. Darby, R. Jagsi, E. L. Lorenzen, O. McArdle, P. McGale, S. Myerson, et al. "A cardiac contouring atlas for radiotherapy", *Radiotherapy and Oncology*, vol. 122 (2017), pp. 416–422.

[9] V. A. van den Bogaard, L. V. van Dijk, R. Vliegenthart, N. M. Sijtsema, J. A. Langendijk, J. H. Maduro, and A. P. Crijns. "Development and evaluation of an auto-segmentation tool for the left anterior descending coronary artery of breast cancer patients based on anatomical landmarks", *Radiotherapy and Oncology*, vol. 136 (2019), pp. 15–20.

[10] E. D. Morris, A. I. Ghanem, M. Dong, M. V. Pantelic, E. M. Walker, and C. K. Glide-Hurst. "Cardiac substructure segmentation with deep learning for improved cardiac sparing", *Medical physics*, vol. 47 (2020), pp. 576–586.

[11] S. Bruns, J. M. Wolterink, R. A. Takx, R. W. van Hamersvelt, D. Suchá, M. A. Viergever, T. Leiner, and I. Išgum. "Deep learning from dual-energy information for whole-heart segmentation in dual-energy and single-energy non-contrast-enhanced cardiac CT", *Medical physics*, vol. 47 (2020), pp. 5048–5060.

[12] R. W. van Hamersvelt, I. Išgum, P. A. de Jong, M. J. M. Cramer, G. E. Leenders, M. J. Willemink, M. Voskuil, and T. Leiner. "Application of speCtraL computed tomograAphy to impRove specIficity of cardiac compuTed tomographY (CLARITY study): rationale and design", *BMJ open*, vol. 9 (2019), p. e025793.

[13] S. Bruns, J. M. Wolterink, R. W. van Hamersvelt, T. Leiner, and I. Išgum. "CNN-based segmentation of the cardiac chambers and great vessels in non-contrast-enhanced cardiac CT", *International Conference on Medical Imaging with Deep Learning*, 2019.

[14] J. M. Wolterink, R. W. van Hamersvelt, M. A. Viergever, T. Leiner, and I. Išgum. "Coronary artery centerline extraction in cardiac CT angiography using a CNN-based orientation classifier", *Medical image analysis*, vol. 51 (2019), pp. 46–60.

[15] A. Sironi, E. Türetken, V. Lepetit, and P. Fua. "Multiscale centerline detection", *IEEE Transactions on Pattern Analysis and Machine Intelligence*, vol. 38 (2015), pp. 1327–1341.

[16] K. He, X. Zhang, S. Ren, and J. Sun. "Deep residual learning for image recognition", *Proceedings of the IEEE conference on computer vision and pattern recognition*, 2016, pp. 770–778.

[17] T. G. Dietterich. "Ensemble methods in machine learning", *International workshop on multiple classifier systems*, Springer. 2000, pp. 1–15.

[18] D. P. Kingma and J. Ba. "Adam: a method for stochastic optimization", *International Conference on Learning Representations*, 2015.

[19] M. Schaap, C. T. Metz, T. van Walsum, A. G. van der Giessen, A. C. Weustink, N. R. Mollet, C. Bauer, H. Bogunović, C. Castro, X. Deng, et al. "Standardized evaluation methodology and reference database for evaluating coronary artery centerline extraction algorithms", *Medical image analysis*, vol. 13 (2009), pp. 701–714.

[20] A. Moignier, D. Broggio, S. Derreumaux, A. Beaudré, T. Girinsky, J.-F. Paul, D. Drubay, D. Lefkopoulos, D. Franck, B. Aubert, et al. "Coronary stenosis risk analysis following Hodgkin lymphoma radiotherapy: a study based on patient specific artery segments dose calculation", *Radiotherapy and Oncology*, vol. 117 (2015), pp. 467–472.

[21] R. Kaderka, E. F. Gillespie, R. C. Mundt, A. K. Bryant, C. B. Sanudo-Thomas, A. L. Harrison, E. L. Wouters, V. Moiseenko, K. L. Moore, T. F. Atwood, et al. "Geometric and dosimetric evaluation of atlas based auto-segmentation of cardiac structures in breast cancer patients", *Radiotherapy and Oncology*, vol. 131 (2019), pp. 215–220.

[22] F. Van Dijk-Peters, N. Sijtsema, R. Kierkels, R. Vliegenthart, J. Langendijk, J. Maduro, and A. Crijns. "Validation of a multi-atlas based auto-segmentation of the heart in breast cancer patients", *Radiotherapy and Oncology*, vol. 115 (2015), pp. S132–S133.

[23] O. Bernard, A. Lalande, C. Zotti, F. Cervenansky, X. Yang, P.-A. Heng, I. Cetin, K. Lekadir, O. Camara, M. A. G. Ballester, et al. "Deep learning techniques for automatic MRI cardiac multi-structures segmentation and diagnosis: is the problem solved?", *IEEE transactions on medical imaging*, vol. 37 (2018), pp. 2514–2525.

[24] W. Tan, L. Xu, X. Wang, D. Qiu, G. Han, and D. Hu. "Estimation of the displacement of cardiac substructures and the motion of the coronary arteries using electrocardiographic gating", *OncoTargets and therapy*, vol. 6 (2013), pp. 1325–1332.

[25] F. A. van Nimwegen, M. Schaapveld, D. J. Cutter, C. Janus, A. Krol, M. Hauptmann, K. Kooijman, J. Roesink, R. van der Maazen, S. C. Darby, et al. "Radiation dose-response relationship for risk of coronary heart disease in survivors of hodgkin lymphoma", *Journal of clinical oncology*, vol. 34 (2016), pp. 235–243.

[26] K. M. Atkins, T. L. Chaunzwa, N. Lamba, D. S. Bitterman, B. Rawal, J. Bredfeldt, C. L. Williams, D. E. Kozono, E. H. Baldini, A. Nohria, et al. "Association of left anterior descending coronary artery radiation dose with major adverse cardiac events and mortality in patients with non-small cell lung cancer", *JAMA oncology*, vol. 7 (2021), pp. 206–219.